Ceramics International 50 (2024) 25228–25240

Contents lists available at ScienceDirect

Ceramics International

journal homepage: www.elsevier.com/locate/ceramint

Effect of milling and compaction on sintering of porcelain stoneware tiles

Sonia Conte, Chiara Molinari *, Michele Dondi, Guia Guarini, Chiara Zanelli

Institute of Science, Technology and Sustainability for the Development of Ceramic Materials CNR-ISSMC - Via Granarolo, 64 48018, Faenza, RA, Italy

ARTICLE INFO

Handling Editor: Dr P. Vincenzini

Keywords:
Particle size distribution
Powder compaction
Sintering
Vitreous phase

ABSTRACT

The present study aims to provide a deeper understanding of how different particle size distributions and degrees of powder compaction affect the densification process of porcelain stoneware tiles. For this purpose, three different batches underwent a laboratory simulation of the industrial tilemaking process, at growing grinding time or increasing forming pressure, with technological characterization of both unfired and fired products. Sintering behaviour was determined by hot-stage microscopy. Phase composition was determined by XRD-Rietveld allowing the estimation of the chemical composition and physical properties of the liquid phase. The results illustrate the impact of too fine (or too coarse) grain size on powder compaction, firing shrinkage, water absorption, efficiency of densification, sintering rate, stability at high temperature, and risk of anticipated overfiring (and similarly for too high or too low forming pressure). Simultaneous variation of particle size and forming pressure beyond usual standards induced changes in technological behaviour that in most cases compensate each other. Phase composition is moderately influenced by particle size and little by powder compaction. The vitreous phase mainly suffered from a decreasing degree of polymerization as the particle size became finer or the dry bulk density decreased. In case of insufficient grinding, too much residual feldspars caused improper composition and properties of the glassy phase, which resulted in lower efficiency of densification and slower sintering rate. Both the sintering kinetics and degree of densification depend on the timescale, i.e. the ratio of surface tension to viscosity (melt) and median particle size. Nevertheless, a low powder compaction can trigger a microstructural effect on sintering (improving both densification rate and efficiency) that may outweigh the timescale effect.

1. Introduction

Porcelain stoneware has become the most popular material in the world in the manufacture of large tiles and ceramic slabs, for which accurate sintering control is a key point in the process to meet geometric and dimensional standards [1]. Although the formulation of porcelain stoneware batches is quite well-known and standardized, there is still a certain flexibility in the batch design allowed by ceramic technology [2–4]. In addition, the worldwide diffusion means that tiles are produced with a wide range of raw materials with different compositional and technological characteristics [5,6]. Despite this undoubted variability of the porcelain stoneware formulations, batches complying with the standard prescriptions for Group BIa (ISO 13006) [7] exhibit a firing behaviour that is generally very similar to each other.

The firing behaviour of porcelain stoneware is mainly governed by the amount and properties of the viscous phase formed at high temperature [8–10]. However, some technological parameters play a key role: conditions of body preparation (in particular the particle size distribution) and pressing (especially the degree of compaction of unfired tiles) turn to be crucial for tile sintering. Deviations from optimal process conditions can significantly affect not only the technological properties (water absorption, firing shrinkage, bulk density, mechanical strength) but also densification kinetics and dimensional stability at maximum firing temperatures, making interpretation of sintering curves difficult or sometimes even misleading.

It is known from previous studies on porcelain stoneware that finer particle size distributions lead to a higher fired bulk density and a lower temperature at which the water absorption target is achieved [11–13]. The sintering kinetics is faster after longer milling [14]. Firing shrinkage increases with fine particle sizes, but this is largely due to the simultaneous decrease in dry bulk density [13]. The dimensional stability at the maximum firing temperature seems to be enhanced in case of finer particle size. In contrast, a coarser particle size and/or a greater amount of feldspar in this coarse fraction results in a less compact

* Corresponding author.
E-mail address: chiara.molinari@issmc.cnr.it (C. Molinari).

https://doi.org/10.1016/j.ceramint.2024.04.253
Received 9 February 2024; Received in revised form 2 April 2024; Accepted 19 April 2024
Available online 23 April 2024

microstructure, favouring the persistence of larger pores in the finished products [12,15]. No data are available on phase composition of fired tiles as the starting grain size varies.

The effect of powder compaction has been less investigated for porcelain stoneware, although it is also influenced by particle size distribution and hence somehow accounted for in the above mentioned studies. An increased dry bulk density of tiles brings about less firing shrinkage and less water absorption, as well as higher bulk density and mechanical strength [16,17]. The final microstructure (and particularly the total porosity after firing) does not vary significantly with the degree of compaction of dry tiles [14,17]. A different dry bulk density does not affect the phase composition of porcelain stoneware, but a variation of the aspect ratio of mullite crystals was observed [17].

From this framework, there is a lack of knowledge on the effect of milling and compaction on phase transformations occurring during the firing of porcelain stoneware, which in turn influence the quantity, composition and physical properties of the liquid phase. Therefore, it is necessary to understand how different particle size distributions and degrees of powder compaction influence the phase composition and the properties of the liquid phase. This is to reliably assess the porcelain stoneware densification process and to have guidelines for the correct interpretation of sintering curves. For this purpose, the same batch was subjected to increasing grinding times or increasing forming pressures, to compare the effect of grain size and powder compaction on the firing behaviour of porcelain stoneware.

1.1. Background

It is known that the sintering of porcelain stoneware occurs by viscous flow and is governed mainly by the physical properties (in particular viscosity and surface tension) of the liquid phase that develops at high temperatures, along with the particle size [9,14]. Such physical properties strictly depend on the temperature and chemical composition of the liquid phase [18,19]. The latter depends in turn on the reactions that occur during firing between the minerals of raw materials [10] according to a given vitrification path [20] that is somehow affected, among other factors, by the grain size and the degree of powder compaction.

As a first approximation, densification kinetics initially follows the Frenkel's model of *neck formation* [21,22]:

$$\frac{\Delta L}{L_0} = \frac{3\,\gamma}{8\,\eta\,r}\,t \qquad \text{(eq. 1)}$$

where L_0 is the length of the sample, ΔL the linear shrinkage at time t, η is the shear viscosity and γ is the liquid-vapor surface tension of the melt, and r the initial radius of the particles. When the relative density becomes approximately higher than 0.8, the process follows the Mackenzie and Shuttleworth's model of *vented bubble* [21,22]:

$$\frac{d\rho}{dt} = \frac{3\gamma}{\eta\,2a}\,\frac{k_2^{1/3}}{2a}(1-\rho)^{2/3}\,\rho^{1/3} \qquad \text{(eq. 2)}$$

where dρ/dt is the densification rate, a is the initial radius of bubbles, and ρ is the relative density. The physical properties of the melt play a relevant role also in the model of *complex relaxation* proposed by Amorós et al. [23]:

$$\alpha = \frac{\varepsilon - \varepsilon_{min}}{\varepsilon_0 - \varepsilon_{min}} = \exp\left[\left(1 - \frac{t}{\bar{\tau}}\right)^n\right] \text{ with } \bar{\tau} = -\frac{9}{4}\,\frac{\gamma}{r\,\eta} \qquad \text{(eq. 3)}$$

where α is the degree of sintering progress, ε is the porosity of the sample at time t, ε_{min} is the minimum porosity and ε_0 is the initial porosity, t is the time, the exponent n varies from 0 to 1, and τ is the characteristic relaxation time.

All the above described models have a term accounting for the ratio of surface tension to shear viscosity of the melt and the starting particle size. Thus, porcelain stoneware batches – once different for grain size and chemical-mineralogical composition – would follow different vitrification paths during firing. Through this process, the derived liquid phases would therefore have distinct physical characteristics that should reflect on a different kinetics of densification, especially in the initial phase (coalescence of viscous droplets). However, when comparing industrial bodies of different composition, we unexpectedly observe initial densification kinetics that are substantially equivalent (Fig. 1).

The observed slopes do not vary according to different ratios of surface tension to viscosity of the liquid phases, but it seems that the densification process is activated when a critical value is reached, in particular in terms of timescale t_s [24]:

$$t_s = \frac{r\,\eta}{\gamma}\,. \qquad \text{(eq. 4)}$$

For the bodies shown in Fig. 1, the timescale ranges from 0.51 to 1.51 s. This critical range of values is reached at a given temperature by each body, and therefore the start of densification is the parameter that can most differentiate porcelain stoneware batches.

The sintering behaviour of the batches differs clearly in the next phase in which there are isolated pores in the melt, to an extent apparently more accentuated than expected based on the vented bubble or relaxation models [22,23]. In the example of Fig. 1B, the sintering rate begins to slow down, at a sample volume between 88 % and 91 %, to eventually attain different degrees of densification. Going on, de-sintering may start by development of closed porosity (the so-called *pore coarsening*) and/or collapse of the ceramic body because the effective viscosity falls below a value that ensures the maintenance of the tile geometry [25].

It is expected that the start of densification depends on the solid load with influence of other factors, like particle size distribution and powder packing [22,26]. On the other hand, it is known that these factors affect the behaviour during firing and can modify the axiom of porcelain stoneware, which wants a very low water absorption (<0.2 %) to be achieved at the same time of maximum densification (Fig. 2A). This implies that the aforementioned phenomena leading to de-sintering have not yet begun. If particle size distribution and/or powder compaction do not respect optimal values, a violation of the axiom can lead to anticipated overfiring [27] with water absorption that reaches the desired value when the bulk density is already decreasing compared to the maximum value (Fig. 2B).

2. Materials and methods

2.1. Materials

Three porcelain stoneware batches were utilized: an industrial batch (M, spray-dried powder) and two laboratory batches (P and C, both reproducing industrial formulations). The chemical composition of these batches is reported in Table A1 (Appendices).

2.2. Lab-scale processing

Batch P was treated to have a sample with particle size distribution equivalent to the industrial benchmark (P1) and three samples with increasingly finer particle size distributions (Fig. 3) within the benchmark (P2 and P3) or slightly over milled (P4). The starting mix of raw materials (lots of 2 kg each) was wet ground by a planetary ball mill (Magellano, Ceramic Instruments, Italy) in porcelain jars with alumina grinding media (water 40 % of the slip, sodium tripolyphosphate 0.3 % of dry weight). Four increasing milling times were set up: 20, 30, 40 and 50 min (P1 to P4, respectively). The slips so obtained were dried in oven at 105 °C overnight, deagglomerated by hammer mill (grid 0.75 mm) and hand granulated (sieve 2 mm, ~6 % water).

Batch C was processed to compare a sample with particle size distribution typical of industrial practice (C0) with a sample with a coarser

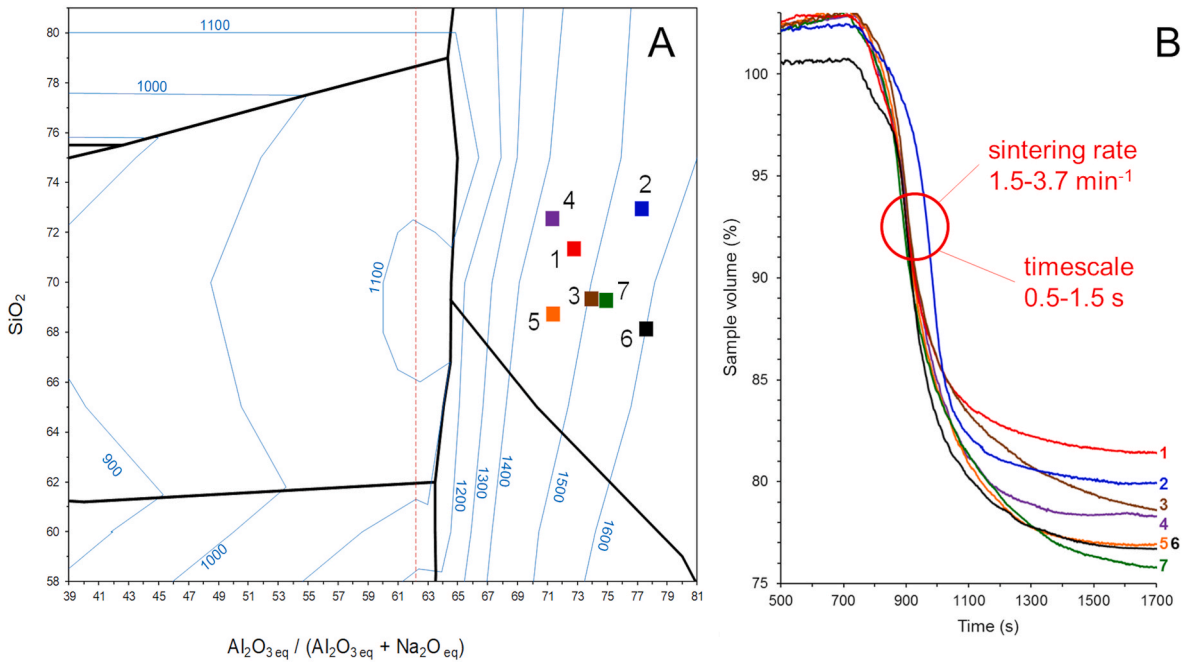

Fig. 1. Composition and firing behaviour of seven porcelain stoneware bodies representative of the industrial production: A) chemical composition plotted in the ternary Na_2O-K_2O-Al_2O_3-SiO_2 diagram (Conte et al., 2020b); B) isothermal sintering curves with observed ranges of densification rate and timescale.

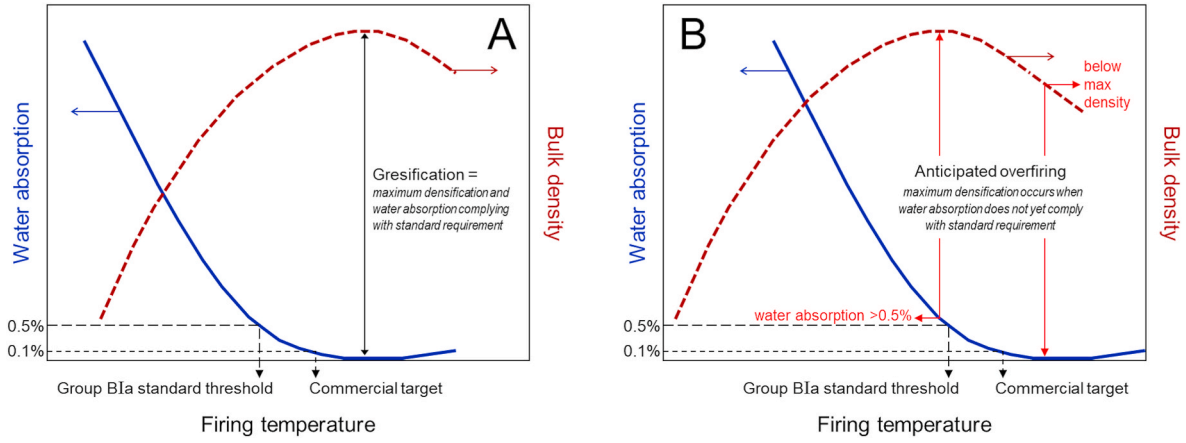

Fig. 2. Firing behaviour of porcelain stoneware bodies: water absorption and bulk density as a function of temperature. A) Axiom of proper gresification. B) Undesired behaviour showing anticipated overfiring (modified after Contartesi [27]).

granulometry (Fig. 3) representative of under milling (CU). The starting mix of raw materials (lots of 1 kg each) was wet ground by a planetary ball mill (Magellano, Ceramic Instruments, Italy) in porcelain jars with alumina grinding media (water 40 % of the slip, sodium tripolyphosphate 0.6 % of dry weight). Two increasing milling times were set up: 8 and 15 min. The slips so obtained were dried in oven at 105 °C overnight, deagglomerated by hammer mill (grid 0.5 mm) and hand granulated adding ~7 % water (sieve 2 mm).

Powders of both C and P batches were compacted with a hydraulic press (40 MPa, Nannetti C800, Italy) into tiles (110 × 55 × 5 mm, length × width × thickness). Differences in the sample load in the ball mill (1 or 2 kg) were due to availability of raw materials. The higher amount of deflocculant in C bodies was necessary due to worse rheological behaviour than P bodies.

Body M: the spray-dried powder was used as received with no milling. Discs (50 × 5 mm, diameter × thickness) were obtained by uniaxial pressing (hydraulic press Nannetti CR, Italy) at four specific pressures: 10, 27, 40 and 60 MPa.

The green compacts of all bodies were dried in an electric oven at 105 °C overnight then fast fired in an electric roller kiln (ER15, Nannetti, Faenza, Italy) with different firing schedules, where T_{max} is the maximum temperature, t_{fir} is the total time (cold-to-cold) and t_{dw} is the dwell time at T_{max}. Batch C: T_{max} 1220 °C, t_{fir} 60 min and t_{dw} 5 min; Body M: T_{max} 1210 °C, t_{fir} 60 min and t_{dw} 6 min; Body P: T_{max} 1220 °C, t_{fir} 51 min and t_{dw} 5 min.

2.3. Technological characterization

Particle size distribution of powders was measured by gravity monitoring of sedimentation (Sedigraph III 5125 plus, Micromeritics, UK) following the ASTM C958 standard [28]. The compaction and drying behaviours were assessed by measuring springback [100 $(L_p\text{-}L_m)/L_m$, where L_p is the length of the pressed tile and L_m is the length of the mold], drying shrinkage [100 $(L_d\text{-}L_p)/L_p$, where L_d is the length of the dry tiles], green and dry bulk density (weight/volume ratio) and bending strength (ISO 10545-4 standard) [29].

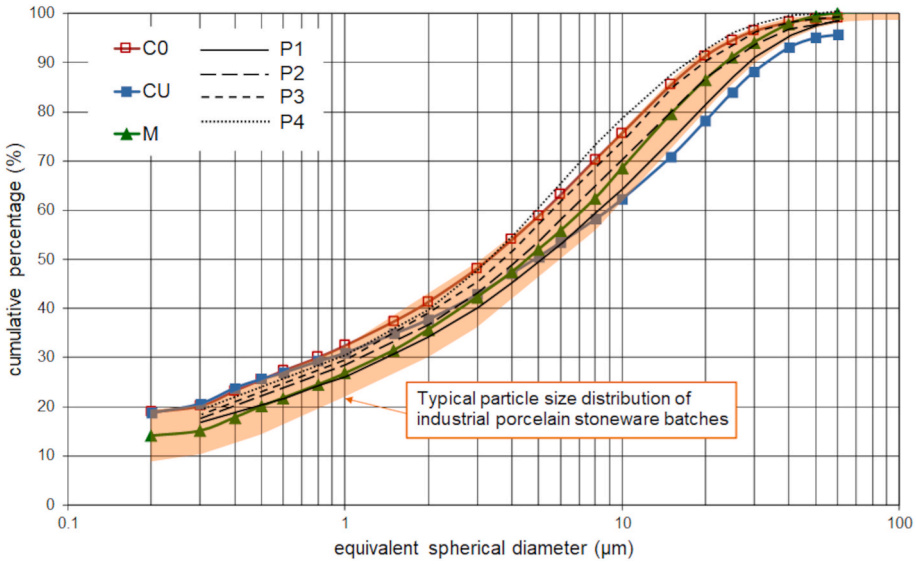

Fig. 3. Particle size distribution of batches M, C (C0 benchmark and CU undermilled) and P (increasing milling times from P1 to P4).

Technological properties determined on five fired specimens were: linear firing shrinkage [100 (L_m–L_f)/L_m where L_f is the length of the fired tiles]; bending strength (ISO 10545–4) [29]; water absorption, bulk density and open porosity (ISO 10545–3) [30]; specific weight by Helium pycnometry (ISO 18753); total porosity [100- (bulk density/specific weight)] and closed porosity = (total-open).

2.4. Sintering behaviour

The sintering behaviour was investigated by in-situ experiments on specimens (approximately 5 × 5 × 5 mm) cut from the dry tiles. Isothermal tests were carried out by optical thermo-dilatometry (TA, ODP868, Germany or Expert Lab Service, Misura, Italy) with a heating ramp of 80 °C/min up to T_{max} (1100, 1150, 1175 and 1200 °C) and 30 min dwell time. Measurement of specimen dimensions (height and area of the silhouette every second) allowed determining the temperature at which densification starts. Furthermore, sintering and coarsening rates were calculated from the variation of sample height and area, respectively, as a function of time. The sintering rate was determined at the neck formation stage, i.e., in the interval between reaching the maximum temperature and the moment in which the height variation deviated from the linear trend. The swelling rate was determined after reaching the maximum density, from the moment swelling began until the end of the test.

2.5. Composition of fired bodies

Quantitative phase analysis (QPA) was performed by X-ray powder diffraction (D8 Advance and LynxEye, Bruker, Germany). Patterns were collected with a Cu X-ray tube (operating at 40 kV and 40 mA) from 10 to 100°2θ, step size of 0.02°2θ, counting time of 1 s per step. Every sample was admixed with 20 wt% corundum (or fluorite) as internal standard for the quantification of crystalline and amorphous phases [31]. The XRPD patterns were modelled by a full profile Rietveld refinement with the GSAS-EXPGUI software package [32,33]. The agreement indices of all refinements were in the following ranges: 8.0 % < R_p < 11.0 %; 10.0 % < R_{wp} <12.0 %; 2.0 < X^2 < 5.5; and 9.0 % < R (F^2) < 11.0 %.

The chemical composition of the vitreous phase was calculated by the difference between the chemical composition of the fired body and the contribution of crystalline phases, assuming their stoichiometric compositions weighted on the QPA [25]. Pseudo-structural parameters of the vitreous phase were calculated on the base of the obtained chemical composition [34].

- *degree of melt depolymerization* (NBO/T, mol%) defined as the number of nonbridging oxygens (NBO) per tetrahedrally-coordinated cations (Si, Al);
- *alumina saturation index* of the melt, ASI (mol%) = Al_2O_3/(Na_2O + K_2O + CaO);
- *charge compensators* that balance the Si^{4+}-Al^{3+} charge mismatch and stabilize Al ions in tetrahedral coordination, CCAT (mol%) = Na + K + 2Ca + 2Mg (up to a maximum value = Al);
- *glass network formers*, GNF (mol%) = Si + CCAT;
- *glass network modifiers*, GNM (mol%) = Na + K + Mg + Ca + Al (exceeding the values of CCAT).

The physical properties at high temperature of the vitreous phase were estimated by predictive models based on its chemical composition. The gas-liquid surface tension was obtained by interpolating the data obtained by Appen's and Dietzel's methods [25], while shear viscosity calculation was based on the Giordano-Russell-Dingwell model [18].

An effective viscosity of the body at high temperature (η_{eff}) was estimated as the product of the relative viscosity (η_{rel}) by the shear viscosity of the melt (η_{melt}): $\eta_{eff} = \eta_{melt} \cdot \eta_{rel}$ [9]. The relative viscosity was calculated by the relation [35]:

$$\eta_{rel} = \left[1 - \frac{\varphi}{\varphi_c}\right]^{-B\varphi_c} \quad \text{(eq. 5)}$$

where φ is the solid load and φ_c is the critical solid fraction (set to 0.72) below which the relative viscosity starts to lower [26].

3. Results and discussion

3.1. Effect of particle size distribution finer than industrial target

The technological behaviour of body P milled to increasingly finer particle size is shown in Table 1.

As the particle size decreased, a reduction in bulk density was found in both the green and dry states, confirming what observed by Darolt et al. [13]. However, the trend could be made more pronounced, for samples P3 and P4, by an accidental slight decrease in the powder moisture. The mechanical strength of green and dry tiles remained substantially within the uncertainty range of measurements. This is apparently in contrast to previous work in which an increasing trend of

Table 1
Technological properties of the P body with different particle size distributions.

Property	unit	P1	P2	P3	P4
Milling time	min	20	30	40	50
Powder median particle size	μm	5.1	4.2	3.7	3.3
Powder moisture	%wt.	6.6 ± 0.1	6.8 ± 0.1	6.4 ± 0.1	6.2 ± 0.1
Pressing springback	$cm \cdot m^{-1}$	0.49 ± 0.01	0.55 ± 0.02	0.55 ± 0.02	0.57 ± 0.01
Green bulk density	$g \cdot cm^{-3}$	1.98 ± 0.01	1.95 ± 0.01	1.90 ± 0.01	1.82 ± 0.01
Green bending strength	MPa	0.52 ± 0.04	0.41 ± 0.01	0.51 ± 0.02	0.47 ± 0.15
Drying shrinkage	$cm \cdot m^{-1}$	−0.09 ± 0.05	−0.07 ± 0.03	−0.14 ± 0.02	−0.13 ± 0.03
Dry bulk density	$g \cdot cm^{-3}$	1.86 ± 0.01	1.82 ± 0.01	1.78 ± 0.01	1.79 ± 0.01
Dry bending strength	MPa	1.13 ± 0.15	1.15 ± 0.06	1.02 ± 0.11	1.09 ± 0.06
Fired bulk density	$g \cdot cm^{-3}$	2.37 ± 0.01	2.37 ± 0.01	2.39 ± 0.01	2.39 ± 0.01
Water absorption	%wt.	0.29 ± 0.02	0.24 ± 0.04	0.09 ± 0.02	0.07 ± 0.04
Open porosity	%vol.	0.7 ± 0.1	0.6 ± 0.1	0.2 ± 0.1	0.2 ± 0.1
Closed porosity	%vol.	3.6 ± 0.4	3.1 ± 0.3	3.1 ± 0.3	3.3 ± 0.3
Total porosity	%vol.	4.3 ± 0.4	3.7 ± 0.4	3.3 ± 0.3	3.5 ± 0.4
Fired bending strength	MPa	38.7 ± 0.7	38.2 ± 0.6	40.7 ± 1.8	38.3 ± 1.8

the modulus of rupture was noted [13]. However, considering that the bulk density of body P became lower as the particle size decreased, a constant mechanical strength is equivalent to an increase at the same compaction degree of the dry tiles.

In the firing stage, finer grain sizes induced a decrease in water absorption and, at the same time, a slight increase (if any) in bulk density. This confirms the observations in the literature [11–13]. No significant variation occurred to the mechanical strength, and this contrasts with the case of anorthite-based stoneware [11]. The variations in bulk density and open porosity, although modest, denote a step between P2 and P3, which reflects marked changes in phase composition: decrease of mullite, feldspars, and quartz, and increase in the vitreous phase (Table 2).

The chemical composition of the vitreous phase, going from P1 to P4, turned increasingly peraluminous (ASI from 1.24 to 1.43) and less polymerized (NBO/T from 0.148 to 0.166) so approaching the field of equilibrium with sample P4 (Fig. 4). The values of glass network formers, modifiers, and charge compensators oscillate within relatively narrow ranges, without clear trends as a function of granulometry. Therefore, viscosity and surface tension of the melt varied little as the grain size decreased. The most marked effect concerns the drop in solid load, which involves a clear reduction in relative viscosity in samples P3 and P4. In terms of effective viscosity, there is a slight decrease with the median diameter of the particles.

The isothermal sintering curves are reported in Figure A1 (Appendices). The sintering rate calculated from them is higher only for sample P4, confirming previous observations [36]. The temperature of densification start decreased as the particle size became finer. This behaviour is in reasonable accordance with the values of timescale estimated from the melt composition. The coarsening rate is similar in all samples (Table 2).

Although the finer particle size increased reactivity during firing (greater involvement of quartz and mullite in the phase transformations) and promoted a slightly faster sintering rate, the effects on deformations at high temperature were much less pronounced than expectable. This is presumably due to a buffering mechanism characteristic of porcelain stoneware [25]: the loss of solid fraction is somehow compensated by the increase in melt viscosity, while the effective viscosity remains essentially unchanged. This mechanism can be perceived when the particle size decreases, as it happened from P2 to P3: quartz decreased from 28 % to 20 %, inducing a drop in relative viscosity from 5.2 to 2.6; the alkali-to-silica ratio of the liquid phase decreased, inducing an increment of melt viscosity from 4.57 to 4.81 log Pa·s; as a result, the effective viscosity has remained virtually constant.

3.2. Effect of particle size distribution coarser than industrial target

The technological behaviour of batch C is shown in Table 3, where the coarse-grained sample CU is compared with the sample C0 (standard

Table 2
Phase composition and sintering behaviour of bodies P and chemical composition, pseudo-structural parameters, and physical properties of the vitreous phase.

		unit	P1	P2	P3	P4
Phase composition	Vitreous phase	%wt.	55.8 ± 3.4	56.7 ± 2.1	70.2 ± 1.9	67.3 ± 2.9
	Quartz	%wt.	25.5 ± 2.4	28.0 ± 1.6	20.4 ± 2.4	25.5 ± 1.9
	Mullite	%wt.	8.8 ± 1.9	10.3 ± 2.4	6.5 ± 1.9	6.0 ± 1.3
	Plagioclase	%wt.	6.8 ± 0.3	4.0 ± 0.1	0.9 ± 0.2	0.4 ± 0.1
	K-feldspar	%wt.	1.6 ± 0.1	0.6 ± 0.1	0.5 ± 0.1	0.5 ± 0.1
	Cristobalite	%wt.	1.5 ± 0.1	0.3 ± 0.1	1.4 ± 0.3	0.3 ± 0.1
Melt chemical composition	SiO_2	%wt.	69.3	69.6	70.1	68.0
	TiO_2	%wt.	1.0	1.0	0.8	0.8
	Al_2O_3	%wt.	17.1	16.2	17.9	19.4
	Fe_2O_3	%wt.	1.0	1.0	0.8	0.9
	MgO	%wt.	0.9	0.9	0.7	0.7
	CaO	%wt.	0.6	0.8	0.7	0.7
	Na_2O	%wt.	6.0	6.5	5.8	6.1
	K_2O	%wt.	4.1	4.0	3.2	3.4
Melt pseudo-structural parameters	NBO/T	%mol.	0.148	0.155	0.158	0.166
	alumina saturation index, ASI	%mol.	1.24	1.33	1.28	1.43
	glass network formers, GNF	%atom	42.2	41.8	42.2	41.7
	charge compensators, CCAT	%atom	9.1	8.6	8.8	9.3
	glass network modifiers, GNM	%atom	0.3	0.9	0.7	1.0
Physical properties at T_{max}	Surface tension (melt)	$N \cdot m^{-1}$	0.329	0.328	0.332	0.335
	Shear viscosity (melt)	$\log_{10}$ Pa·s	4.66	4.57	4.81	4.68
	Timescale (melt)	s	0.71	0.48	0.72	0.47
	Relative viscosity (body)	1	5.55	5.20	2.60	2.97
	Effective viscosity (body)	$\log_{10}$ Pa·s	5.29	5.18	5.19	5.11
Sintering behaviour	Sintering rate at 1200 °C	min^{-1}	2.9	2.6	2.8	3.8
	Coarsening rate at 1200 °C	min^{-1}	0.02	0.02	0.04	0.03
	Efficiency of densification	%	95.7	96.3	96.7	96.5
	Starting of densification	°C	1116	1115	1086	1043

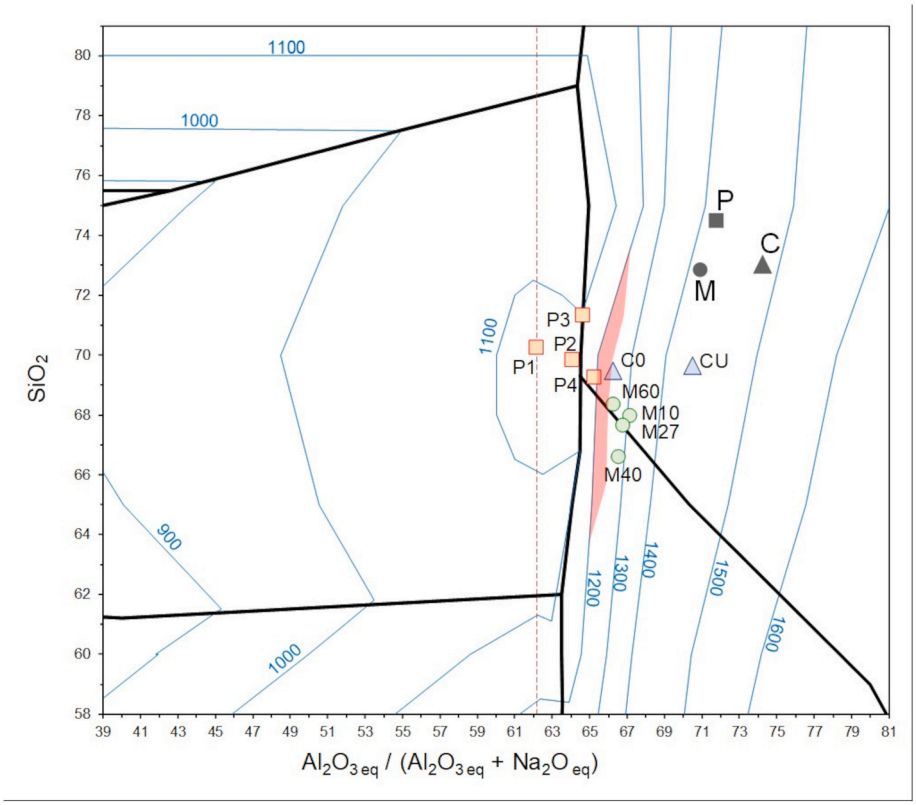

Fig. 4. Chemical composition of batches C, M and P and corresponding vitreous phases plotted in the Na_2O_{eq}-Al_2O_{3eq}-SiO_2 system. The area in red colour represents the compositional field of melts in thermodynamic equilibrium at firing temperatures around 1200 °C. (For interpretation of the references to colour in this figure legend, the reader is referred to the Web version of this article.)

Table 3
Technological properties of batch C milled to a particle size distribution of the industrial practice (C0) and under milled to a coarser particle size (CU).

Property	Unit	CU	C0
Milling time	Min	8	15
Powder median particle size	Mm	5.0	3.2
Powder moisture	%wt.	7.1 ± 0.1	7.5 ± 0.1
Pressing springback	$cm \cdot m^{-1}$	0.41 ± 0.02	0.50 ± 0.02
Green bulk density	$g \cdot cm^{-3}$	2.162 ± 0.003	2.066 ± 0.003
Drying shrinkage	$cm \cdot m^{-1}$	0.04 ± 0.01	0.04 ± 0.01
Dry bulk density	$g \cdot cm^{-3}$	2.018 ± 0.003	1.936 ± 0.003
Firing maximum temperature	°C	1220	1220
Fired bulk density	$g \cdot cm^{-3}$	2.293 ± 0.001	2.350 ± 0.002
Firing shrinkage	$cm \cdot m^{-1}$	4.0 ± 0.2	5.5 ± 0.3
Water absorption	%wt.	0.8 ± 0.1	0.1 ± 0.1
Open porosity	%vol.	1.9 ± 0.2	0.3 ± 0.1

particle size distribution).

The undermilled body (CU) exhibits much higher values than C0 of both green and dry bulk density. This confirms what has already been noted by Amorós et al. [12]: a less sorted particle size distribution allows for a more efficient powder compaction with a lower springback.

The firing behaviour is clearly different: the insufficient degree of grinding (CU) led to a serious loss of bulk density associated with a water absorption value trespassing the standard threshold (Fig. 5A). This undesirable behaviour resembles what is referred to as *anticipated overfiring* [27]. The shrinkage of CU is lower than that of C0, largely because of the dry bulk density values. However, the difference in the porosity of dry tiles is about 3 %, which would account for 1 % shrinkage only, the rest is due to less efficient densification of sample CU, resulting in more porosity in the fired tile.

The less efficient densification of CU compared to C0 was confirmed by sintering curves (Fig. 5B). The different firing behaviour is clearly reflected in the phase composition: CU has a high content of unreacted feldspars and consequently a relatively low amount of glassy phase (Table 4). There is less mullite in CU, while the quartz content is practically the same. This different vitrification degree directly affects the composition of the liquid phase, which appears very different in CU with respect to C0, which is close to the equilibrium field (Fig. 4). The melt of the undermilled sample CU appears to be strongly peraluminous (ASI 1.5 versus 1.2 of C0) as well as less polymerized (NBO/T 0.20 versus 0.17 of C0). In pseudo-structural terms, the liquid phase of CU has slightly less formers (GNF) and charge compensators (CCAT) but twice the amount of modifiers (GNM), essentially represented by Al^{3+}. The higher melt viscosity, together with the greater solid load, justifies the slower sintering rate and the lower efficiency of densification. The higher effective viscosity of CU explains why this body has a lower tendency to deform at high temperature, as demonstrated by a lower coarsening rate.

These results show, in case of under milling, that a high amount of unreacted fluxes can be present, leading to improper composition and physical properties of the melt, which in turn cause inefficient sintering. Such behaviour is similar to the effect of feldspars in the coarse grain fraction of porcelain stoneware tiles [15].

3.3. Effect of variable degree of powder compaction

The technological behaviour of body M is shown in Table 5. The main effect of increasing pressure, in both green and dry tiles, is a greater bulk density, as expected [16,37]. In the firing stage, the increasing powder compaction allowed to reach a lower water absorption and, at the same time, an improved bulk density. The firing shrinkage decreased by increasing the forming pressure and is inversely proportional to the dry bulk density, confirming what found by Pérez and Romero [17]. The dry tiles have an estimated open porosity ranging

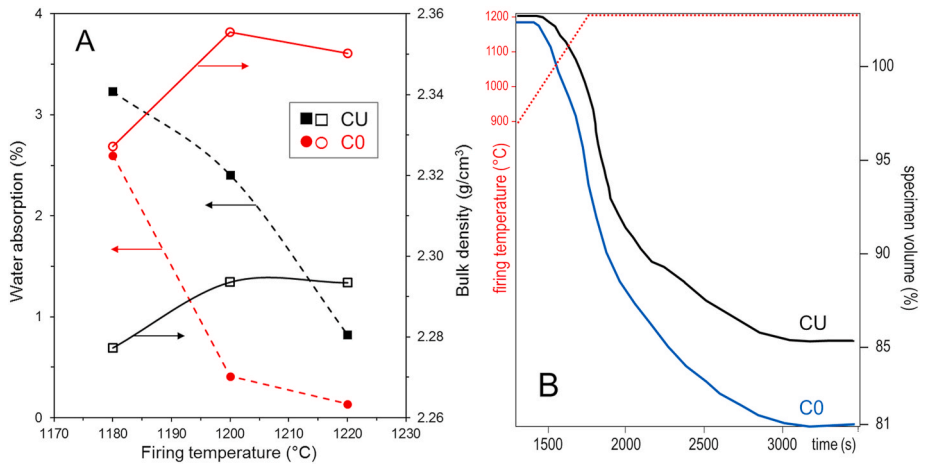

Fig. 5. Firing behaviour of batch C: A) gresification curves in the 1180–1220 °C range; B) isothermal sintering curves (ramp 40 °C/min to 1200 °C).

Table 4
Phase composition and sintering behaviour of bodies C and chemical composition, pseudo-structural parameters, and physical properties of the vitreous phase.

		unit	CU	C0
Phase composition	Vitreous phase	%wt.	46.9 ± 0.3	65.2 ± 0.4
	Quartz	%wt.	22.5 ± 0.2	22.9 ± 0.1
	Mullite	%wt.	7.1 ± 0.1	8.6 ± 0.2
	Plagioclase	%wt.	20.2 ± 0.1	2.0 ± 0.1
	K-feldspar	%wt.	3.3 ± 0.1	1.4 ± 0.2
Melt chemical composition	SiO_2	%wt.	66.8	68.1
	TiO_2	%wt.	1.4	1.0
	Al_2O_3	%wt.	21.1	19.5
	Fe_2O_3	%wt.	1.2	0.9
	MgO	%wt.	0.8	0.6
	CaO	%wt.	1.0	0.7
	Na_2O	%wt.	3.8	6.1
	K_2O	%wt.	3.9	3.3
Melt pseudo-structural parameters	NBO/T	%mol.	0.202	0.175
	alumina saturation index, ASI	%mol.	1.49	1.19
	glass network formers, GNF	%atom	40.5	41.4
	charge compensators, CCAT	%atom	8.4	8.9
	glass network modifiers, GNM	%atom	2.8	1.4
Physical properties at 1220 °C	Surface tension (melt)	$N \cdot m^{-1}$	0.340	0.335
	Shear viscosity (melt)	$\log_{10}$ Pa·s	4.93	4.74
	Timescale (melt)	s	1.25	0.52
	Relative viscosity (body)	1	6.66	3.28
	Effective viscosity (body)	$\log_{10}$ Pa·s	5.62	5.20
Sintering behaviour	Sintering rate at 1200 °C	min^{-1}	2.88	3.24
	Coarsening rate 1200 °C	min^{-1}	0.04	0.06
	Efficiency of densification	%	92.5	95.2
	Starting of densification	°C	942	943

from 34.3 % (M10) to 26.7 % (M60). The difference between pressing at 10 and 60 MPa is 7.6 % in volume and should correspond to about 2.5 % of linear shrinkage, which is less than what experimentally determined

Table 5
Technological properties of body M compacted at increasing pressure.

Property	unit	M10	M27	M40	M60
Specific pressure	MPa	10	27	40	60
Powder median particle size	μm	4.4	4.4	4.4	4.4
Powder moisture	%wt.	4.0	4.0	4.0	4.0
Pressing springback	$cm \cdot m^{-1}$	0.71 ± 0.02	0.79 ± 0.02	0.86 ± 0.02	0.84 ± 0.02
Green bulk density	$g \cdot cm^{-3}$	1.767 ± 0.003	1.900 ± 0.003	1.926 ± 0.003	1.967 ± 0.003
Drying shrinkage	$cm \cdot m^{-1}$	−0.08 ± 0.02	−0.12 ± 0.02	−0.05 ± 0.02	−0.10 ± 0.02
Dry bulk density	$g \cdot cm^{-3}$	1.739 ± 0.003	1.864 ± 0.003	1.892 ± 0.003	1.939 ± 0.003
Total porosity (dry)	%vol.	34.3 ± 0.2	29.5 ± 0.2	28.5 ± 0.2	26.7 ± 0.2
Fired bulk density	$g \cdot cm^{-3}$	2.357 ± 0.002	2.363 ± 0.002	2.376 ± 0.002	2.387 ± 0.002
Firing shrinkage	$cm \cdot m^{-1}$	10.2 ± 0.2	9.0 ± 0.2	7.5 ± 0.2	7.2 ± 0.2
Water absorption	%wt.	0.15 ± 0.01	0.09 ± 0.01	0.08 ± 0.01	0.01 ± 0.01
Open porosity	%vol.	0.36 ± 0.02	0.22 ± 0.02	0.18 ± 0.02	0.02 ± 0.02

(3.0 %).

Indeed, the gain in bulk density after firing between M60 and M10, as low as 0.03 g cm^{-3}, is clearly less than the starting difference, as the dry bulk density gap was 0.20 g cm^{-3}. This means that a lower powder compaction is largely recovered during firing, as already found in the literature [17,37].

Phase composition did not vary significantly for different forming pressures, as already observed by Pérez and Romero [17]. Only quartz fluctuate in a wider range, because it is slightly more abundant in M40 (Table 6). The chemical composition of the vitreous phase is therefore very similar in all samples, with close values of alumina saturation index (~1.2) and degree of de-polymerization (NBO/T ~0.18). There are just small differences in terms of silica content and $Al_2O_{3eq}/(Na_2O_{eq} + Al_2O_{3eq})$ ratio, which see the melt composition approaching the equilibrium field for forming pressure of 40 MPa or higher (Fig. 4). Pseudo-structural parameters are practically the same, without any trend as a function of applied pressure. Consequently, the values of surface tension and viscosity of the melt are similar, with small variations due essentially to the slight differences in the silica amount.

The sintering curves are practically superimposed for all samples in the initial stage of neck formation, but a marked difference regards the start of the vented bubble stage (Fig. 6A) as well as the efficiency and

Table 6
Phase composition and sintering behaviour of bodies M and chemical composition, pseudo-structural parameters, and physical properties of the vitreous phase.

		Unit	M10	M27	M40	M60
Phase composition	Vitreous phase	%wt.	70.0 ± 0.7	70.6 ± 0.5	64.1 ± 0.9	68.1 ± 0.4
	Quartz	%wt.	20.4 ± 0.3	21.6 ± 0.3	24.0 ± 0.6	20.8 ± 0.2
	Mullite	%wt.	5.1 ± 0.3	4.8 ± 0.2	5.2 ± 0.3	5.4 ± 0.1
	Plagioclase	%wt.	4.1 ± 0.2	2.6 ± 0.3	5.4 ± 0.3	5.0 ± 0.2
	K-feldspar	%wt.	0.4 ± 0.1	0.4 ± 0.2	1.3 ± 0.3	0.7 ± 0.1
Melt chemical composition	SiO_2	%wt.	67.1	66.4	65.3	67.1
	TiO_2	%wt.	1.0	0.9	1.0	1.0
	Al_2O_3	%wt.	20.3	20.8	21.4	20.2
	Fe_2O_3	%wt.	0.9	0.9	1.0	0.9
	MgO	%wt.	0.3	0.3	0.4	0.4
	CaO	%wt.	1.3	1.3	1.4	1.4
	Na_2O	%wt.	6.6	6.8	6.9	6.6
	K_2O	%wt.	2.5	2.5	2.5	2.5
Melt pseudo-structural parameters	NBO/T	%mol.	0.177	0.182	0.180	0.174
	alumina saturation index, ASI	%mol.	1.21	1.22	1.21	1.19
	glass network formers, GNF	%atom	41.3	41.0	41.0	41.3
	charge compensators, CCAT	%atom	9.3	9.4	9.7	9.3
	glass network modifiers, GNM	%atom	1.5	1.6	1.6	1.3
Physical properties at T_{max}	Surface tension (melt)	$N \cdot m^{-1}$	0.342	0.343	0.344	0.342
	Shear viscosity (melt)	$\log_{10}$ Pa·s	4.85	4.81	4.74	4.85
	Timescale (melt)	s	0.91	0.83	0.70	0.91
	Relative viscosity (body)	1	2.64	2.57	3.46	2.87
	Effective viscosity (body)	$\log_{10}$ Pa·s	5.24	5.19	5.23	5.26
Sintering behaviour	Sintering rate at 1200 °C	min^{-1}	2.40	2.04	2.19	2.07
	Coarsening rate 1200 °C	min^{-1}	0.02	0.05	0.08	0.07
	Efficiency of densification	%	98.5	95.6	94.8	94.0
	Starting of densification	°C	1030	1023	1014	1014

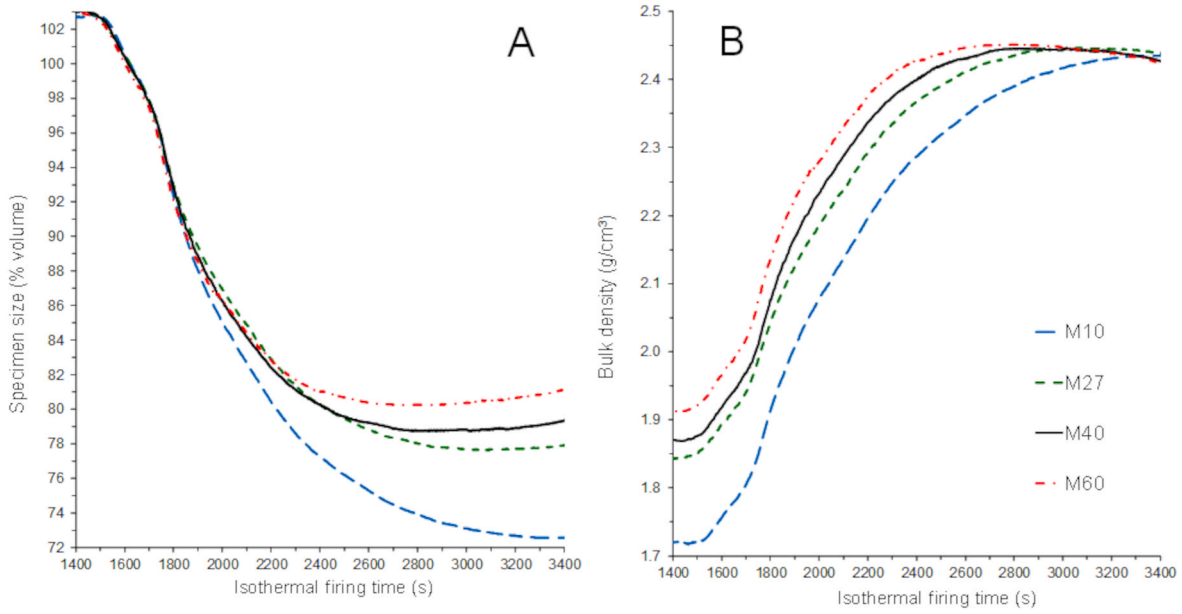

Fig. 6. Isothermal sintering curves by HSM at 1200 °C of body M compacted at increasing pressure: A) specimen volume, and B) bulk density, as a function of firing time.

starting of densification (Table 6). Although sintering kinetics are very similar, dry tiles with lower bulk density shrank more and at a slightly faster rate, eventually achieving a greater efficiency of densification (Fig. 6B). As if having more starting porosity, where the liquid phase can expand, could allow for faster densification kinetics. In other words, there seems to be an effect of microstructure on sintering kinetics, which takes over the physical properties of the liquid phase (when there are no substantial differences in quantity and chemical composition of the melt).

3.4. Discussion

A milling process carried out to a particle size different from usual values in the industrial practice brings about various repercussions (for the same forming pressure). Opposite effects emerge if the particle size is finer (series P) or coarser (series C) with respect to the benchmark (Table 7). The rate of variation of the technological parameters as a function of the median diameter of the particles is rather high.

Powder compaction carried out at a forming pressure lower than the industrial target (for the same particle size distribution) leads to various changes in behaviour (series M). The effects of a forming pressure higher than the reference value are essentially the opposite (Table 7). The rate

Table 7
Effect of different degrees of milling or compaction on the technological behaviour and sintering process of porcelain stoneware tiles with respect to the industrial benchmark.

Property	Too fine particle size (series P)	Too coarse particle size (series C)	Too low forming pressure (series M)	Too high forming pressure (series M)
Powder compaction	Worse	better	too low	too high
Firing shrinkage	More	less	more	less
Degree of vitrification	higher	lower	~ unchanged	~ unchanged
Vitreous phase composition	minor changes	important changes	~ unchanged	~ unchanged
Vitreous phase properties	minor changes	important changes	~ unchanged	~ unchanged
Sintering rate	faster	slower	slightly faster	slightly slower
Water absorption	less	more	more	less
Efficiency of densification	~ unchanged	less	more	less
Stability at high temperature	slightly less	slightly more	slightly more	slightly less
Risk of anticipated overfiring	low	high	~ unchanged	more

of variation of the technological parameters as a function of the forming pressure is low.

Although some convergence can be observed in the impacts on technological properties, there is no overall correspondence between the effects of particle size and powder compaction. This implies that simultaneously varying grain size and forming pressure beyond usual standards (e.g., too fine particle size together with too high forming pressure) can generate enhancing effects on only some properties (e.g., lowering the water absorption) since the remaining ones exhibit variations that tend to compensate each other. Indeed, joint changes in grinding and compaction do not bias against the overall technological behaviour of porcelain stoneware bodies.

Limited changes occurred to phase composition or chemical and physical characteristics of the glassy phase. This means that variations of particle size or powder compaction do not radically alter the vitrification path. Considering all samples together, it can be appreciated that the amount of vitreous phase tends to grow and to turn increasingly less polymerized, as particle size becomes finer or the dry bulk density decreases (Fig. A2).

In general, both the efficiency of densification and sintering kinetics of porcelain stoneware are inversely correlated to the timescale of the liquid phase (Fig. 7) with two outliers. The first exception is sample CU, where the insufficient grinding left an excessive amount of coarse-grained feldspars, which led to an unfavourable composition of the glassy phase – poorly polymerized and far from the thermodynamic equilibrium field – which translated in a low efficiency of densification and a slower sintering rate.

The second exception is sample M10, which exhibits a more efficient densification than expectable based on its timescale. To justify this behaviour, a microstructural effect can be envisaged, as if there were a factor, proportional to the volume of the starting porosity, which could enhance the sintering kinetics. In any case, the degree of powder packing is confirmed as determining factor to start the densification process, as there is an inverse relationship with the bulk density of dry tiles (Fig. 8A). However, the timescale also influences the start of sintering (Fig. 8B), which implies a relationship with viscosity and surface tension of the liquid phase, but also with granulometry (since the two out-of-trend samples, C0 and P4, are the ones with the finest particle size).

4. Conclusions

The present study provides a deeper understanding of how different particle size distributions and degrees of powder compaction influence the densification process of porcelain stoneware tiles, with new insights into the effects on composition, properties and role of the liquid phase.

- A too fine particle size leads to a worse powder compaction, causing a higher firing shrinkage and sintering rate but without significant changes in the efficiency of densification and a slightly worse stability at high temperature. For particle size distribution excessively coarse the opposite behaviour is observed, with a higher risk of anticipated overfiring.
- The increase of pressure in the shaping step, higher than the industrial values, induces a greater powder compaction, reducing firing shrinkage, sintering rate and water absorption. At the same time, lower efficiency of densification and slightly worse stability at high temperature are observed with a tendence to anticipate overfiring. Opposite effects were found when a much lower forming pressure was adopted.
- Simultaneous variation of particle size and forming pressure generate changes in technological behaviour that tend to compensate each other.
- Phase composition is moderately affected by particle size and powder compaction. The chemical composition and physical properties

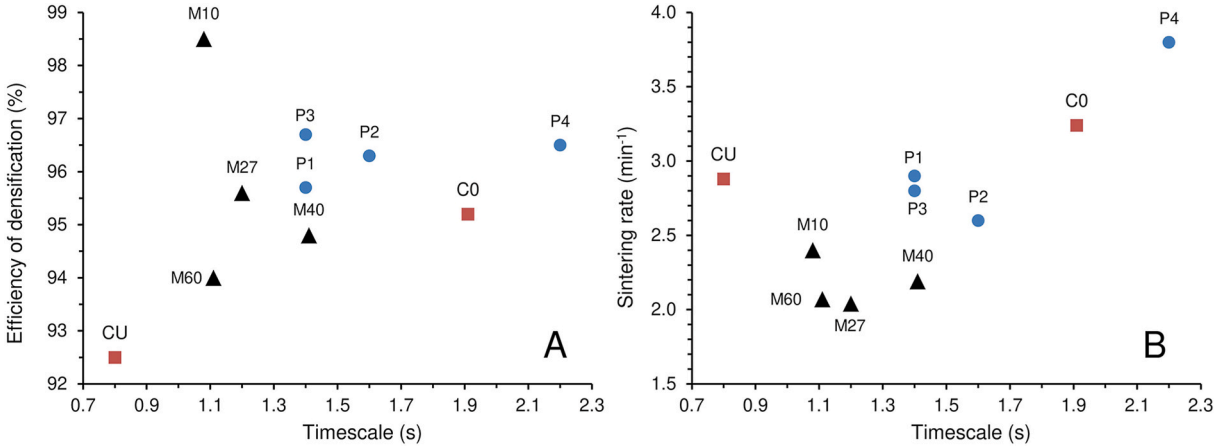

Fig. 7. Firing behaviour as a function of timescale of the liquid phase: A) efficiency of densification and B) sintering rate.

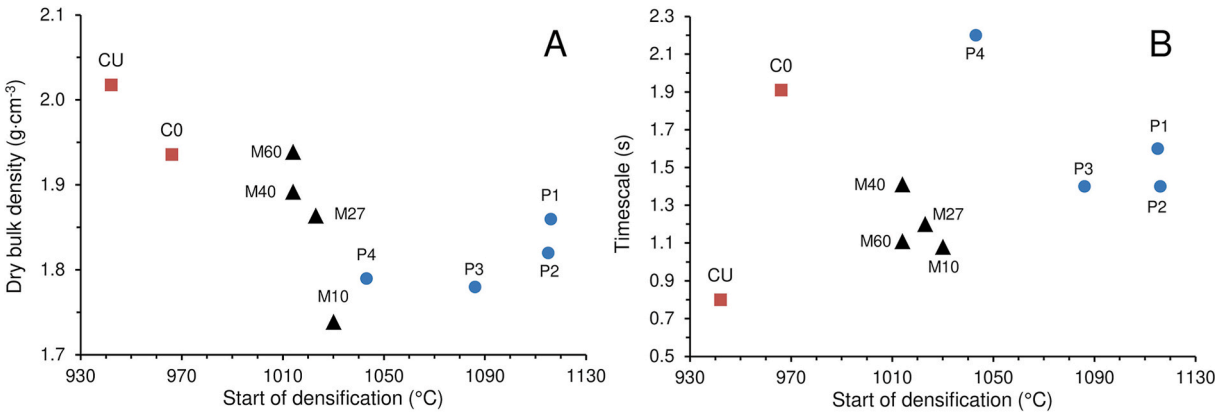

Fig. 8. Temperature at which densification starts as a function of powder compaction (A) or timescale of the liquid phase (B).

of the vitreous phase exhibit minor changes. Lower particle size and bulk density lead to higher vitrification degree and decrease in melt polymerization. Only in case of insufficient grinding (which led to an excessive amount of coarse-grained feldspars) a deviation in glassy phase composition and properties was found, lowering densification efficiency and sintering rate.

Both the sintering kinetics and densification efficiency depend on the timescale of the liquid phase (ratio of viscosity and median particle size to surface tension). However, a large porosity of dry tiles can trigger a microstructural effect on sintering kinetics, that takes over the timescale (when there are no substantial differences in the liquid phase properties).

Declaration of interests

The authors declare that they have no known competing financial interests or personal relationships that could have appeared to influence the work reported in this paper.

One of the authors (Michele Dondi) is an Editorial Board Member for Ceramics International and was not involved in the editorial review or the decision to publish this article.

CRediT authorship contribution statement

Sonia Conte: Conceptualization, Data curation, Writing – original draft, Writing – review & editing. **Chiara Molinari:** Conceptualization, Data curation, Writing – original draft, Writing – review & editing. **Michele Dondi:** Conceptualization, Data curation, Investigation, Methodology, Validation, Writing – original draft, Writing – review & editing. **Guia Guarini:** Formal analysis. **Chiara Zanelli:** Project administration, Supervision, Writing – review & editing.

Acknowledgements

This study was funded by the ECOSISTER project (ECS00000033, CUP B89I22000650001) under the National Recovery and Resilience Plan (PNRR), Mission 04 Component 2 Investment 1.5, funded by the European Union —NextGenerationEU, Call for tender n. 3277 dated December 30, 2021 Award Number: 0001052 dated June 23, 2022.

Appendices.

Table A1
Chemical composition of batches

%wt.	P	C	M
SiO_2	73.89	69.77	71.90
TiO_2	0.54	0.60	0.67
Al_2O_3	17.50	18.87	18.72
Fe_2O_3	0.58	0.54	0.62
MgO	0.49	0.35	0.24
CaO	0.58	0.44	0.92
Na_2O	4.16	4.03	5.08
K_2O	2.27	2.25	1.84

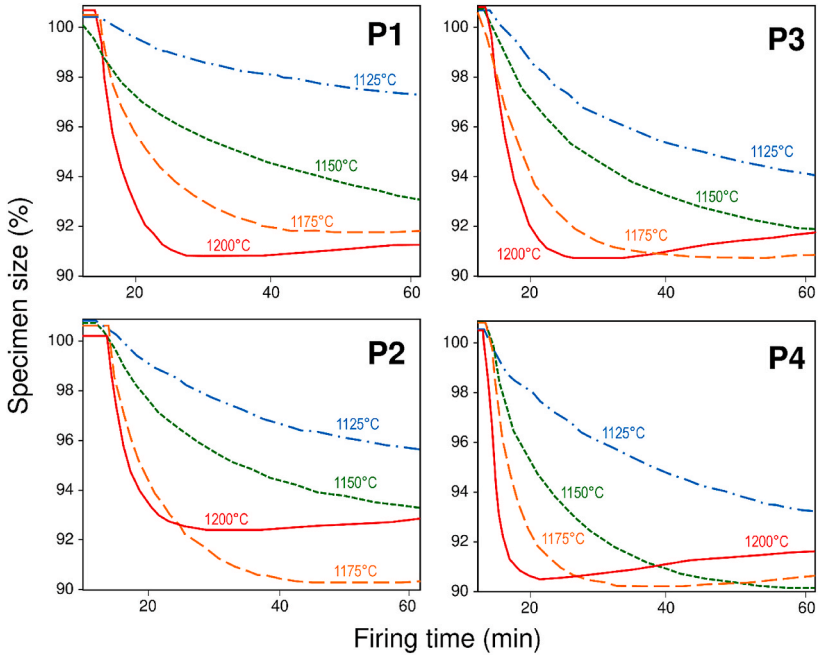

Fig. A1. Sintering curves by HSM of body P milled to increasing finer particle size distribution.

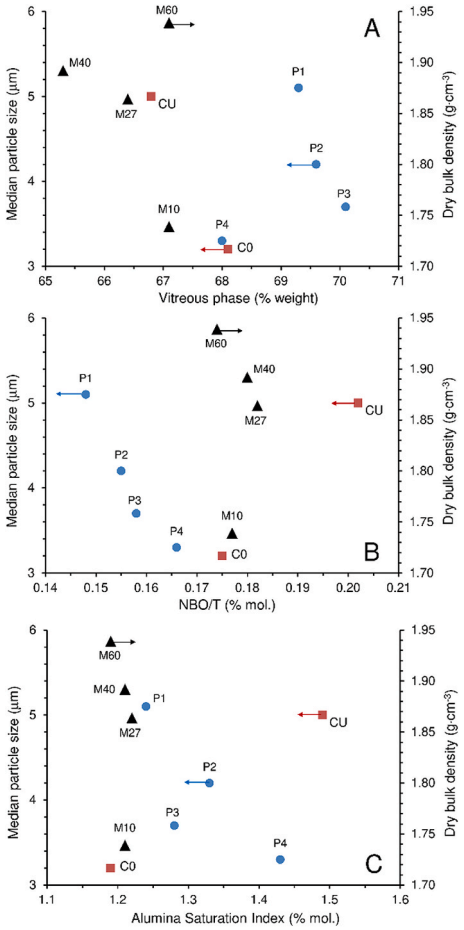

Fig. A2. Degrees of vitrification (A), depolymerization (B) and alumina saturation of the melt, as a function of particle size distribution (series C and P) or degree of powder compaction (Series M).

References

[1] J.P. Junior, A. Zaccaron, S. Arcaro, J.B.R. Neto, A. de Noni Junior, F.R. Pereira, Novel approach to ensure the dimensional stability of large-format enameled porcelain stoneware tiles through water absorption control, Open Ceram 9 (2022) 100203.

[2] M. Dondi, M. Raimondo, C. Zanelli, Clays and bodies for ceramic tiles: reappraisal and technological classification, Appl. Clay Sci. 96 (2014) 91–109.

[3] A.D.N. Junior, S.B. Canever, P. Henrique, R.R. da Silva, Microstructure-oriented porcelain stoneware tile composition design, Ceram. Int. 49 (14) (2023) 24558–24565.

[4] M. Zamani, H. Yapicioglu, A. Kara, C. Sevik, Statistical analysis of porcelain tiles' technical properties: full factorial design investigation on oxide ratios and temperature, Phys. Scripta 98 (2023) 125953.

[5] M. Dondi, M. Vicent-Cabedo, E. Rambaldi, C. Zanelli, J. García-Ten, Raw material flows in the European ceramic tile industry: case study of Italy and Spain, 16th World Congress on Ceramic Tile Quality, QUALICER (2020) 10–11. Castellón (Spain).

[6] C.T. Brasileiro, S. Conte, F. Contartesi, F.G. Melchiades, C. Zanelli, M. Dondi, A. O. Boschi, Effect of strong mineral fluxes on sintering of porcelain stoneware tiles, J. Eur. Ceram. Soc. 41 (11) (2021) 5755–5767.

[7] ISO 13006, Ceramic Tiles. Definitions, Classification, Characteristics and Marking, 2018.

[8] S. Salem, A. Salem, Mechanisms of momentum transport in viscous flow sintering, Sci. Sinter. 1 (2013) 287–318.

[9] S. Conte, C. Zanelli, M. Ardit, G. Cruciani, M. Dondi, Phase evolution during reactive sintering by viscous flow: disclosing the inner workings in porcelain stoneware firing, J. Eur. Ceram. Soc. 40 (2020) 1738–1752.

[10] J.L. Amorós, E. Blasco, A. Moreno, C. Feliu, Kinetics of the transformations occurring during the firing process of an industrial spray-dried porcelain stoneware body, Ceram. Int. 48 (2022) 17611–17620.

[11] M.U. Taskiran, N. Demirkol, A. Capoglu, Influence of mixing/milling on sintering and technological properties of anorthite based porcelainised stoneware, Ceram. Int. 32 (2006) 325–330.

[12] J.L. Amorós, M.J. Orts, J. García-Ten, A. Gozalbo, E. Sánchez, Effect of the green porous texture on porcelain tile properties, J. Eur. Ceram. Soc. 27 (2007) 2295–2301.

[13] R.D. Darolt, M. Cargnin, M. Peterson, A. De Noni Jr Additional high-energy milling to enhance the performance of porcelain stoneware manufacturing, Int. J. Appl. Ceram. 17 (2020) 1742–1751.

[14] S. Salem, A. Salem, Effects of technical factors on dimensional stability of porcelain stoneware body during sintering process: isothermal kinetic study, Part II, Thermochim. Acta 598 (2014) 82–90.

[15] H.J. Alves, M.R. Freitas, F.G. Melchiades, A.O. Boschi, Dependence of surface porosity on the polishing depth of porcelain stoneware tiles, J. Eur. Ceram. Soc. 31 (2011) 665–671.

[16] J.M. Pérez, J.M. Rincón, M. Romero, Effect of moulding pressure on microstructure and technological properties of porcelain stoneware, Ceram. Int. 38 (2012) 317–325.

[17] J.M. Pérez, M. Romero, Microstructure and technological properties of porcelain stoneware tiles moulded at different pressures and thicknesses, Ceram. Int. 40 (2014) 1365–1377.

[18] D. Giordano, J.K. Russell, D.B. Dingwell, Viscosity of magmatic liquids: a model, Earth Planet Sci. Lett. 271 (2008) 123–134.

[19] F.B. Wadsworth, J. Vasseur, E.W. Llewellin, J. Schauroth, K.J. Dobson, B. Scheu, D. B. Dingwell, Sintering of viscous droplets under surface tension, Proc. Math. Phys. Eng. Sci. 472 (2016) 20150780.

[20] S. Conte, C. Molinari, M. Ardit, G. Cruciani, M. Dondi, C. Zanelli, Porcelain versus porcelain stoneware: so close, so different. Sintering kinetics. Phase evolution, and vitrification paths, Materials 16 (2023) 171.

[21] M.O. Prado, E.D. Zanotto, R. Müller, Model for sintering polydispersed glass particles, J. Non-Cryst. Solids 279 (2001) 169–178.

[22] F.B. Wadsworth, J. Vasseur, E.W. Llewellin, D.B. Dingwell, Hot sintering of melts, glasses and magmas, Rev. Mineral. Geochem. 87 (2022) 801–840.

[23] J.L. Amorós, E. Blasco, C. Feliu, A. Moreno, Densification of irregular polydispersed glass particles described as a complex relaxation process, Open Ceram 9 (2022) 100205.

[24] J. Vasseur, F.B. Wadsworth, Y. Lavallée, K.U. Hess, D.B. Dingwell, Volcanic sintering: timescales of viscous densificationand strength recovery, Geophys. Res. Lett. 40 (2013) 5658–5664.

[25] S. Conte, C. Zanelli, M. Ardit, G. Cruciani, M. Dondi, Predicting viscosity and surface tension at high temperature of porcelain stoneware bodies: a methodological approach, Materials 11 (2018) 2475.
[26] A. Costa, L. Caricchi, N. Bagdassarov, A model for the rheology of particle-bearing suspensions and partially molten rocks, Geochem. Geophys. 10 (2009) Q03010.
[27] F. Contartesi, F.G. Melchiades, A.O. Boschi, Anticipated overfiring in porcelain tiles: effects of the firing cycle and green bulk density. Bol. Soc. Esp, Ceram. Vidr. 58 (2019) 69–76.
[28] ASTM C958-92, Standard Test Method for Particle Size Distribution of Alumina or Quartz by X-Ray Monitoring of Gravity Sedimentation, 2022.
[29] ISO 10545-4, Ceramic Tiles - Part 4: Determination of Modulus of Rupture and Breaking Strength, 2019.
[30] ISO 10545-3, Ceramic Tiles - Part 3: Determination of Water Absorption, Apparent Porosity, Apparent Relative Density and Bulk Density, 2018.
[31] A.F. Gualtieri, V. Riva, A. Bresciani, S. Maretti, M. Tamburini, A. Viani, Accuracy in quantitative phase analysis of mixtures with large amorphous contents. The case of stoneware ceramics and bricks, J. Appl. Crystallogr. 47 (2014) 835–846.
[32] A.C. Larson, R.B. Von Dreele, GSAS: General Structure Analysis System Report LAUR 86-748, Los Alamos National Laboratory, 1986. Los Alamos, NM.
[33] B.H. Toby, EXPGUI, a graphical user interface for GSAS, J. Appl. Crystallogr. 34 (2001) 210–213.
[34] S. Conte, C. Zanelli, C. Molinari, G. Guarini, M. Dondi, Glassy wastes as feldspar substitutes in porcelain stoneware tiles: thermal behaviour and effect on sintering process, Mater. Chem. Phys. 256 (2020) 123613.
[35] I.M. Krieger, T.J. Dougherty, A mechanism for non-Newtonian flow in suspensions of rigid spheres, Trans. Soc. Rheol. 3 (1959) 137–152.
[36] S. Salem, A. Salem, Shrinkage prediction during non-isothermal sintering in the presence liquid phase: new kinetic model, Part I, Thermochim. Acta 575 (2014) 322–330.
[37] R. Soldati, C. Zanelli, G. Guarini, A. Piancastelli, C. Melandri, S. Fazio, M. C. Bignozzi, M. Dondi, Pore evolution and compaction behaviour of spray-dried bodies for porcelain stoneware slabs, J. Eur. Ceram. Soc. 38 (2018) 4127–4136.